Microfluidic Assembly

DOI: 10.1002/anie.201208324

Continuous Multistep Microfluidic Assisted Assembly of Fluorescent, Plasmonic, and Magnetic Nanostructures**

*Natalia Hassan, Valérie Cabuil, and Ali Abou-Hassan**

In recent years, microfluidics has emerged as an attractive technology for nanocrystal synthesis.[1] This is less true in the field of self-assembly, as limited numbers of nanostructures and microstructures were obtained from molecular building blocks using microfluidic devices.[2] Nevertheless, microfluidic devices allow to achieve superior levels of control of self-assemblies, leading to higher-order structures because self-assembly events are strongly dependent on factors such as the local concentration of reagents, the mixing rates, and the shear forces, which can be finely tuned in a microfluidic device.[2,3] Added to that, such devices make possible a minimal consumption of building blocks, reduced reaction times, the capability for parallel processing, and the ability to perform multi-step synthesis.[4,5]

We report here for the first time, a proof of concept for the continuous multistep microfluidic assisted self-assembly of fluorescent, plasmonic, and magnetic nanostructures to produce lab-on-a-particle architectures.[5–7] Inorganic nanoparticles (Nps) are attractive building block components for the construction of such architectures as their physical and chemical properties can be easily adjusted.[5] Among them, silica nanoparticles (SiO_2 Nps), gold nanoparticles (Au Nps), and the so-called SPIONS (Super-Paramagnetic Iron Oxide Nanoparticles, such as γ-Fe_2O_3 Nps) are very promising materials. Fluorescent silica Nps are widely used because they are easy to produce and have many applications in the field of imaging.[5,8] Gold nanoparticles are used because of their unique optical and electrical properties (e.g. surface plasmon resonance) and their easy functionalization with biological molecules.[5] SPIONS are used as contrast agents for magnetic resonance imaging (MRI), for drug delivery, and as biosensors.[5,9] Indeed, the combination of these different nanoscale materials is a challenge and leads to the development of multifunctional lab-on-a-particle nanoplatforms.[10,11]

The proposed approach for the assembly of nanoparticles is illustrated in Scheme 1. It is based on a continuous multistep process that enables sequential assemblies without leaving the microfluidic environment. The system is made of two glass microreators (μR1 and μR2) with two inlets and one outlet that can operate independently or in synergy. Because of the small dimensions of the microreactors, the two miscible fluids form laminar flows with well-defined mixing between the laminar streams. By varying the flow rates of the colloidal suspensions (or mixing inside every microreactor) diffusive mixing at the boundaries of the streams occurs, thus tuning the pathway of the Np assembly. In μR1 we chose to assemble SiO_2*-Au architectures from the self-assembly of fluorescent silica SiO_2* and Au Nps building blocks while in μR2, γ-Fe_2O_3 magnetic Nps were chosen to attach onto the former nanostructures.

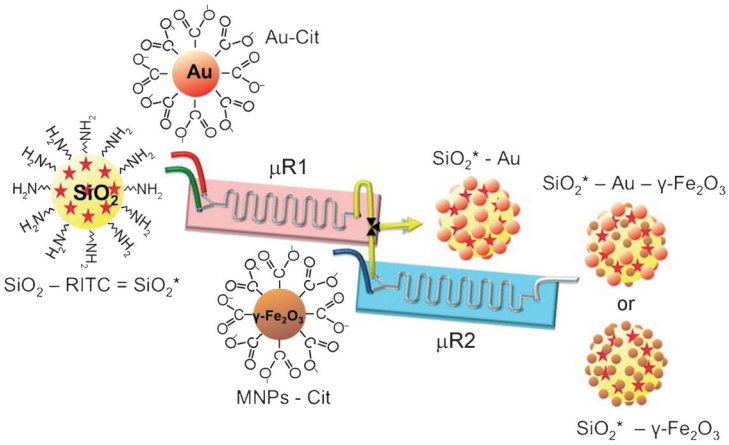

Scheme 1. A two-step microfluidic synthetic procedure for the assembly of multifunctional nanoparticles/fluorescent silica sphere assemblies. RITC = Rhodamine isothiocyanate, Cit = citrate.

In μR1, a colloidal dispersion of SiO_2* Nps modified with (3-aminopropyl)trietoxysilane (APTES) was injected in one of the two inlets of the channel with a flow rate Q_{SiO_2*}, while a solution of citrated coated Au Nps was injected in the second inlet, with a flow rate Q_{Au}. The 186 ± 3 nm diameter silica nanoparticles were synthesized by the typical Stöber method and the organic fluorophore rhodamine isothiocyanate (RITC) was incorporated in their structure to make them fluorescent.[12] The 16.5 ± 3.3 nm diameter citrated gold Nps were synthesized by the modified Turkevich method.[13] At the outlet of μR1 a stable suspension of the obtained SiO_2*-Au nanostructures was continuously injected in one inlet of μR2. In the same time a stable suspension of 5.5 ± 1.2 nm

[*] Dr. N. Hassan, Prof. V. Cabuil, Dr. A. Abou-Hassan
UPMC Université Paris 6, Laboratoire de Physicochimie des Electrolytes Colloïdes et Sciences Analytiques (PECSA)
UMR 7195, équipe Colloïdes Inorganiques
Université Paris 6 (UPMC) Bat F(74), case 51
4 place Jussieu, 75252 Paris Cedex 05 (France)
E-mail: ali.abou_hassan@upmc.fr
Homepage: http://www.pecsa.upmc.fr

[**] We acknowledge funding from the Émergence-UPMC-2011. We thank Dr. Sophie Neveu and Aude Michel from PECSA lab for the TEM images.

Supporting information for this article is available on the WWW under http://dx.doi.org/10.1002/anie.201208324.

citrate-coated γ-Fe_2O_3 nanoparticles (MNPs-Cit) was prepared as described previously by our group[15] was injected in the second inlet of μR2 (see the Supporting Information for TEM images of the different building blocks). Prior to this second step the carbonyl groups of the citrate-coated MNps were activated with 1-ethyl-3-(3-dimethylaminopropyl)carbodiimide hydrochloride (EDC) and *N*-hydroxysuccinimide (NHS) to increase the efficiency of their amide formation with the amine-functionalized silica particles.[15]

After assembling SiO_2* and Au nanostructures in μR1, the assemblies were collected at the exit of the microreactor and analyzed by transmission electron microscopy (TEM) and UV/Vis spectroscopy as shown in Figure 1. We did not proceed to any quenching at the exit of the microreactor.

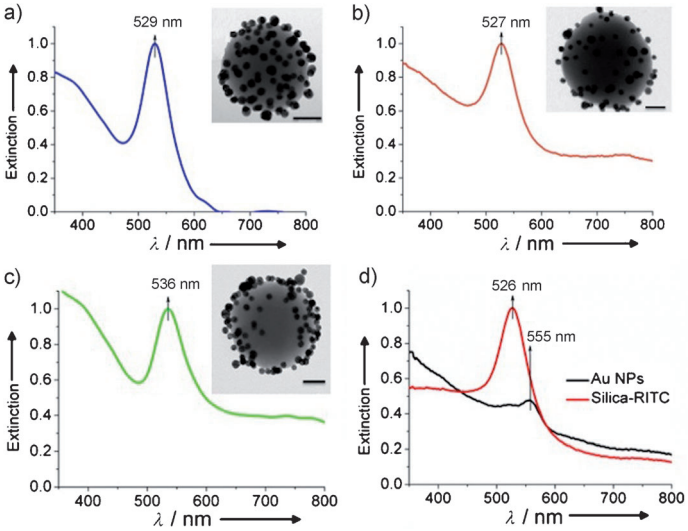

Figure 1. UV/Vis extinction spectrum and representative TEM images (inset) of SiO_2*-Au nanoparticles assembled using different flow rate ratios $\alpha = Q_{Au}/Q_{SiO_2*}$ in the microfluidic device: a) $\alpha = 2.5$ and $t_R = 1.8$ min, b) $\alpha = 1$ and $t_R = 1.8$ min, and c) $\alpha = 2.5$ and $t_R = 0.8$ min. d) UV/Vis extinction spectrum of Au and fluorescent silica SiO_2* nanoparticles before their assembly, the later showing an absorption peak at 555 nm because of the absorption of the RITC molecules. The scale bars in the TEM images are 50 nm. More representative TEM images are provided in the Supporting Information.

Indeed several control experiments of the emerging flow in 1M cold NaCl solution showed the same results as when the flow was collected for five minutes without quenching. By varying the flow rates of the Au and SiO_2* nanoparticle dispersions, we obtained different gold coverages on the silica surfaces as illustrated in the TEM images (insets of Figure 1a, b and c, see the Supporting Information for more images). Also the surface plasmon wavelength shifted from 526 nm (for the free Au nanoparticles) to higher wavelengths (for the Au Nps assembled on the surface of SiO_2*). In agreement with reported works, the distance between the Au Nps on the silica surface decreased with the red shift.[16,17] We observed that the electrostatic interactions between SiO_2* and Au Nps are sufficiently strong so that the SiO_2*-Au nanostructures remained unchanged during centrifugation and following redispersion using ultrasonication.[16] The percentage of gold nanoparticles attached to the surface of the silica Nps varied from 20 to 40% and was evaluated from gold(III) atomic absorption spectroscopy of the supernatant after centrifugation of the samples (please refer to the Supporting Information for more details). When the residence time (t_R) was kept constant and the ratio of the flow rates of the Au Nps to SiO_2* ($\alpha = Q_{Au}/Q_{SiO_2*}$) was decreased the number of Au Nps on the surface of the silica decreased. The same tendency was observed when α was kept constant and the residence time t_R was decreased. Nevertheless when the residence time was decreased dramatically, the Au Nps showed a tendency to segregate on the surface of the silica Nps (Figure 1c) and at the same time the distance between the gold nanoparticles decreased. We rationalized our observations considering the difference in the velocities of both fluids and the diffusion rate of the Au and SiO_2* nanoparticles during mixing by interdiffusion (see the Supporting Information for more details). In brief, varying the flow rates of the different nanoparticles will alter their mass transfer during mixing. The transport of the colloidal nanoparticles will govern the final structures, that is, the number and the preferential attachment of the gold nanoparticles on the surface of the silica. Also, the difference in the velocities during mixing of the silica and the gold Nps induces a shear at the interface that may organize the Au Nps before they get assembled on the silica surface. These effects were observed by simulations for suspension of nanoparticles flowing on rotating surface and experimentally in microfluidic systems for directed assembly of one-dimensional nanostructures on the microchannel wall.[18,19] Different theoretical works support the possibility to drive out of equilibrium a suspension of nanoparticles by the application of shear flow.[20] Further investigations using numerical simulations to understand and model these observations are in progress.

We studied also the assembly of SiO_2* and γ-Fe_2O_3 in a microreactor similar to μR2. Figure 2 shows the TEM images of SiO_2*-γ-Fe_2O_3 assemblies synthesized in a microreactor similar to μR2 by changing the ratio of the flow rates $\beta = Q_{\gamma\text{-}Fe_2O_3}/Q_{SiO_2*}$. When $Q_{\gamma\text{-}Fe_2O_3}$ was increased a high percentage of MNps covered the silica surface (Figure 2a). The percentage of MNps attached to the surface of the silica Nps varied from 60 to 80% as shown by atomic absorption analysis of the supernatant after centrifugation of the samples. Fluorescence optical microscopy images (Figure 2d) of the SiO_2*-γ-Fe_2O_3 nanostructures confirmed the successful assembly. In the presence of a magnetic field the assemblies aligned along the magnetic field direction and formed chainlike structures (Figure 2e). Compared to the SiO_2*-Au assemblies, the assembly of SiO_2*-γ-Fe_2O_3 nanostructures (Figure 2a to c) is only affected by the ratio of the flow rates (β) and not by the residence time. These differences in Au and MNps assemblies can be mainly explained by the difference in the size of the MNps (5.5 nm γ-Fe_2O_3 compared to 16.5 nm Au Nps). In brief the time necessary to make the two kinds of particles meet is shorter in the case of SiO_2* and γ-Fe_2O_3 Nps than in the case of SiO_2* and Au Nps. For the later the time necessary for the assembly

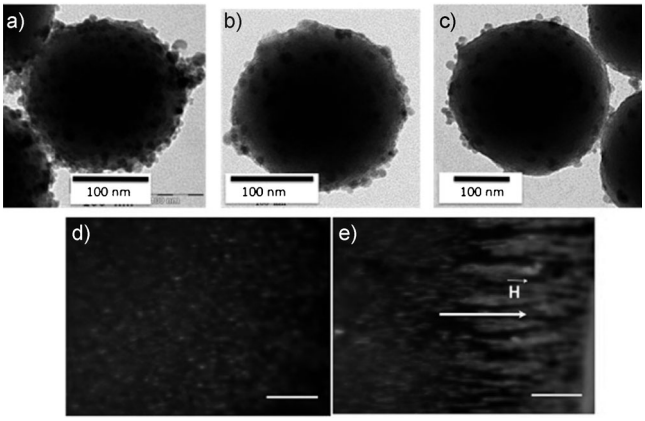

Figure 2. Representative TEM images of SiO_2*-γ-Fe_2O_3 nanostructures synthesized at different flow rates $\beta = Q_{\gamma-Fe_2O_3}/Q_{SiO_2}*$ and the same residence time $t_R = 130$ s; a) $\beta = 10$, b) $\beta = 0.8$, and c) $\beta = 0.5$. Fluorescence optical microscope images of SiO_2*-γ-Fe_2O_3 nanostructures d) in the absence of a magnetic field and e) in the presence of a magnetic field. The scale bars in (d) and (e) are 10 μm ($\vec{H}$ is the direction of the magnetic field). More representative TEM images are provided in the Supporting Information.

is of the same order of magnitude as the residence times in the microreactor (about a minute).

TEM images of extensively washed SiO_2*-Au-γ-Fe_2O_3 nanoparticles (Figure 3a and c) obtained after continuous coupling of μR1 and μR2 to self-assemble in a first step the SiO_2* and Au nanoparticles and get in a second step the SiO_2*-Au-γ-Fe_2O_3 nanostructures are shown in Figure 3a and c. They demonstrate the successful assembly of the multifunctional fluorescent, plasmonic, and magnetic nanostructures. Because of the difference in the electronic contrast and in the size of the MNPs (5.5 nm) and Au Nps (16.5 nm), a zoom on the particles surface (Figure 3b) allowed easily to discriminate between both nanoparticles. The MNPs filled the interstitial space in between the gold nanoparticles on the surface of the silica nanoparticles and a dense coverage of both Au and γ-Fe_2O_3 is observed. The assembly was also confirmed by UV/Vis spectroscopy (Figure 3e). A surface red-shifted plasmon peak appeared, in the spectra of SiO_2*-γ-Fe_2O_3 nanoparticles. EDX characterization showed that the assemblies contain the three diagnostic elements of the precursors, Fe, Si, and Au (see Figure S6 in the Supporting Information). The most MNPs were attached on preformed SiO_2*-Au assemblies when the number of Au Nps on the silica surface was low. This agrees with a mechanism driven by electrostatic attraction. The attachment of γ-Fe_2O_3 on SiO_2*-Au nanostructures was found to depend on the residence time. This residence time has to be compared to the time necessary for the negatively charged MNPs to adsorb on the silica surface, when the latter is sub-saturated with the negatively charged Au Nps. This rate depends intricately on the interactions between the incoming MNPs and the Au Nps previously adsorbed on the surface of silica.

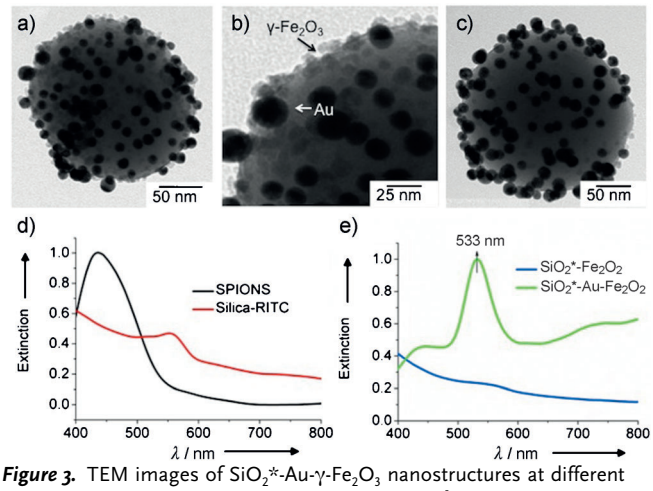

Figure 3. TEM images of SiO_2*-Au-γ-Fe_2O_3 nanostructures at different flow rates, a) $Q_{Au}/Q_{SiO_2}* = 1$, $Q_{\gamma-Fe_2O_3} = 1$ μL min^{-1}, and $t_R = 1.2$ min. b) Enlargement of image (a). c) $Q_{Au}/Q_{SiO_2}* = 1$, $Q_{\gamma-Fe_2O_3} = 5$ μL min^{-1}, and $t_R = 2.2$ min. d) UV/Vis absorbance spectrum of SiO_2* and SPIONS nanoparticles. e) UV/Vis absorbance spectrum of SiO_2*-γ-Fe_2O_3 and SiO_2*-Au-γ-Fe_2O_3 nanostructures for comparison.

We compared the obtained assemblies of SiO_2*-Au, SiO_2*-MNps, and SiO_2*-Au-γ-Fe_2O_3 obtained by using the microfluidic process to the assemblies that can be obtained in bulk. The different building blocks were allowed to assemble under the same conditions of volumetric ratio, concentrations, and residence times as in the microreactor (see Figure S7 in the Supporting Information). We could not obtain the same control over the assemblies in bulk such as in the microfluidic process. Short residence times as those used in the microfluidic process (about a minute) showed a very poor number of Au Nps (about 3%) covering the surface of the silica nanoparticles, even when the relative concentration of Au to SiO_2* was increased. For SiO_2*-MNps and SiO_2*-Au-γ-Fe_2O_3 assemblies, the silica surface was always completely covered with the MNps independently from the residence time or the ratio of the MNps to SiO_2*, thus it was very difficult to control the number of attached MNps by using the microfludic device. All these results demonstrate clearly the advantages of using microfluidic reactors relative to the bulk materials for the assembly as different parameters can be quickly tuned to obtain the desired structures.

In conclusion we have shown a proof of concept for the self-assembly of multifunctional lab-on-a-particle nanostructures from different inorganic building blocks under continuous flow by coupling two microfluidic devices. Fluorescent, plasmonic, and superparamagnetic nanoparticles were self-assembled to obtain multifunctional architectures. Beside the reproducibility of the results and the simplicity of the microfluidic assembly process, the time of assembly was reduced from several hours for the bulk materials to a few minutes (one to two minutes) because of the several advantages offered by the small dimensions of the microdevices. Also, this method is versatile and can be easily generalized and applied to assemble any type of inorganic nanoparticles. Nanostructure self-assemblies in microfluidic devices are dynamic and their kinetics are controlled by the hydrodynamic conditions. Therefore variable assemblies induced by mixing and kinetically trapped in the microdevice can be obtained. These results not only confirm the high potential of microfluidics in materials sciences but open new fundamental perspectives in the use of microfluidic devices

and laminar flows to study and control the kinetics of self-assembly processes. Thus it should be possible from these experimental studies with the help of numerical simulations to find the best parameters such as the size and charge of the nanoparticles, the shear flow, and the residence time, to control on demand the assembly of nanostructures. Therefore different symmetrical and asymmetrical architectures can be assembled and constructed under flow such as Janus nanostructures.

Experimental Section

Synthesis of RITC-doped silica cores: Silica nanoparticles were prepared by a variation of the typical Stöber-based synthesis method changing FITC for RITC.[12] Details of the synthesis are found in the Supporting Information.

Synthesis of MNps (maghemite γ-Fe_2O_3): According to a procedure already described,[14] superparamagnetic γ-Fe_2O_3 nanocrystals were prepared by alkaline co-precipitation of $FeCl_3$ (27%, VWR) and $FeCl_2{\cdot}4H_2O$ (VWR) salts by alkaline solution of tetramethyl ammonium hydroxide $(CH_3)_4NOH$ (97%, Sigma Aldrich). Details can be found in the Supporting Information.

Synthesis of the Au NPs: Gold nanoparticles with a diameter of 16.5 nm were prepared using the modified Turkevich method.[13] More details of the synthesis can be found in the Supporting Information.

Microreactors: The Y-shaped glass microreactors (part number FC_R150.676.2 chip) were purchased from Micronit Microfluidics BV. The dimensions provided by Micronit are: width = 150 μm, height = 150 μm, and length = 0.7 m. Outlet tubes (inner diameter 150 μm, length = 14 cm) were purchased from Polymicro to connect the different microreactors.

Received: October 16, 2012
Revised: December 17, 2012
Published online: January 14, 2013

Keywords: fluorescence · microfluidics · microreactors · nanoparticles · self-assembly

[1] a) J. H. Jung, T. J. Park, S. Y. Lee, T. S. Seo, *Angew. Chem.* **2012**, *124*, 5732 – 5735; *Angew. Chem. Int. Ed.* **2012**, *51*, 5634 – 5637; b) Y. Roig, S. Marre, T. Cardinal, C. Aymonier, *Angew. Chem.* **2011**, *123*, 12277 – 12280; *Angew. Chem. Int. Ed.* **2011**, *50*, 12071 – 12074; c) P. H. Hoang, H. Park, D.-P. Kim, *J. Am. Chem. Soc.* **2011**, *133*, 14765 – 14770; d) S. Marre, K. F. Jensen, *Chem. Soc. Rev.* **2010**, *39*, 1183 – 1202; e) S. Duraiswamy, S. A. Khan, *Nano Lett.* **2010**, *10*, 3757 – 3763; f) A. Abou-Hassan, O. Sandre, V. Cabuil, *Angew. Chem.* **2010**, *122*, 6408 – 6428; *Angew. Chem. Int. Ed.* **2010**, *49*, 6268 – 6286.

[2] a) J. Zhang, R. J. Coulston, S. T. Jones, J. Geng, O. A. Scherman, C. Abell, *Science* **2012**, *335*, 690 – 694; b) C.-W. Wang, D. Sinton, M. G. Moffitt, *J. Am. Chem. Soc.* **2011**, *133*, 18853 – 18864; c) G. Schabas, H. Yusuf, M. G. Moffitt, D. Sinton, *Langmuir* **2008**, *24*, 637 – 643; d) G. Schabas, C.-W. Wang, A. Oskooei, H. Yusuf, M. G. Moffitt, D. Sinton, *Langmuir* **2008**, *24*, 10596 – 10603; e) N. Malmstadt, M. A. Nash, R. F. Purnell, J. J. Schmidt, *Nano Lett.* **2006**, *6*, 1961 – 1965; f) J. L. Steinbacher, R. W. Y. Moy, K. E. Price, M. A. Cummings, C. Roychowdhury, J. J. Buffy, W. L. Olbricht, M. Haaf, D. T. McQuade, *J. Am. Chem. Soc.* **2006**, *128*, 9442 – 9447.

[3] K. J. M. Bishop, C. E. Wilmer, S. Soh, B. A. Grzybowski, *Small* **2009**, *5*, 1600 – 1630.

[4] R. L. Hartman, J. P. McMullen, K. F. Jensen, *Angew. Chem.* **2011**, *123*, 7642 – 7661; *Angew. Chem. Int. Ed.* **2011**, *50*, 7502 – 7519.

[5] J. I. Park, Z. Nie, A. Kumachev, A. I. Abdelrahman, B. P. Binks, H. A. Stone, E. Kumacheva, *Angew. Chem.* **2009**, *121*, 5404 – 5408; *Angew. Chem. Int. Ed.* **2009**, *48*, 5300 – 5304.

[6] A. Burns, H. Ow, U. Wiesner, *Chem. Soc. Rev.* **2006**, *35*, 1028 – 1042.

[7] S. I. Stoeva, F. Huo, J.-S. Lee, C. A. Mirkin, *J. Am. Chem. Soc.* **2005**, *127*, 15362 – 15363.

[8] J. Kim, J. E. Lee, J. Lee, Y. Jang, S.-W. Kim, K. An, J. H. Yu, T. Hyeon, *Angew. Chem.* **2006**, *118*, 4907 – 4911; *Angew. Chem. Int. Ed.* **2006**, *45*, 4789 – 4793.

[9] J. L. Vivero-Escoto, R. C. Huxford-Phillips, W. Lin, *Chem. Soc. Rev.* **2012**, *41*, 2673 – 2685.

[10] a) Z. Nie, A. Petukhova, E. Kumacheva, *Nat. Nanotechnol.* **2010**, *5*, 15 – 25; b) N. C. Bigall, W. J. Parak, D. Dorfs, *Nano Today* **2012**, *7*, 282 – 296.

[11] J. Kim, S. Park, J. E. Lee, S. M. Jin, J. H. Lee, I. S. Lee, I. Yang, J.-S. Kim, S. K. Kim, M.-H. Cho, T. Hyeon, *Angew. Chem.* **2006**, *118*, 7918 – 7922; *Angew. Chem. Int. Ed.* **2006**, *45*, 7754 – 7758.

[12] a) A. Van Blaaderen, A. Vrij, *Langmuir* **1992**, *8*, 2921 – 2931; b) C. Wu, J. Zheng, C. Huang, J. Lai, S. Li, C. Chen, Y. Zhao, *Angew. Chem.* **2007**, *119*, 5489 – 5492; *Angew. Chem. Int. Ed.* **2007**, *46*, 5393 – 5396.

[13] H. Xia, S. Bai, J. Hartmann, D. Wang, *Langmuir* **2010**, *26*, 3585 – 3589.

[14] R. Massart, *IEEE Trans. Magn.* **1981**, *17*, 1247 – 1248.

[15] A. Abou-Hassan, R. Bazzi, V. Cabuil, *Angew. Chem.* **2009**, *121*, 7316 – 7319; *Angew. Chem. Int. Ed.* **2009**, *48*, 7180 – 7183.

[16] S. L. Westcott, S. J. Oldenburg, T. R. Lee, N. J. Halas, *Langmuir* **1998**, *14*, 5396 – 5401.

[17] S. L. Westcott, S. J. Oldenburg, T. R. Lee, N. J. Halas, *Chem. Phys. Lett.* **1999**, *300*, 651 – 655.

[18] O. Koike, S. Ohta, M. Fujita, Y. Yamaguchi, *Jpn. J. Appl. Phys.* **2008**, *47*, 8124 – 8130.

[19] Y. Huang, X. Duan, q. Wei, C. M. Lieber, *Science* **2001**, *291*, 630 – 633.

[20] a) X. Qiu, H. D. Ou-Yang, D. J. Pine, P. M. Chaikin, *Phys. Rev. Lett.* **1988**, *61*, 2554 – 2557; b) R. Besseling, E. R. Weeks, A. B. Schofield, W. C. K. Poon, *Phys. Rev. Lett.* **2007**, *99*, 028301.

